Active Structured Learning for Cell Tracking: Algorithm, Framework and Usability

Xinghua Lou[1,2], Martin Schiegg[1], and Fred A. Hamprecht[1]

[1]Heidelberg Collaboratory for Image Processing (HCI), Interdisciplinary Center for Scientific Computing (IWR), University of Heidelberg, Heidelberg 69115, Germany,

`firstname.lastname@iwr.uni-heidelberg.de`

[2]Computational Biology Center, Memorial Sloan-Kettering Cancer Center, New York, NY 10065, United States

Abstract

One distinguishing property of life is its temporal dynamics, and it is hence only natural that time lapse experiments play a crucial role in modern biomedical research areas such as signaling pathways, drug discovery or developmental biology. Such experiments yield a very large number of images that encode complex cellular activities, and reliable automated cell tracking emerges naturally as a prerequisite for further quantitative analysis. However, many existing cell tracking methods are restricted to using only a small number of features to allow for manual tweaking. In this paper, we propose a novel cell tracking approach that embraces a powerful machine learning technique to optimize the tracking parameters based on user annotated tracks. Our approach replaces the tedious parameter tuning with parameter learning and allows for the use of a much richer set of complex tracking features, which in turn affords superior prediction accuracy. Furthermore, we developed an active learning approach for efficient training data retrieval, which reduces the annotation effort to only 17%. In practical terms, our approach allows life science researchers to inject their expertise in a more intuitive and direct manner. This process is further facilitated by using a glyph visualization technique for ground truth annotation and validation. Evaluation and comparison on several publicly available benchmark sequences show significant performance improvement over recently reported approaches. Code and software tools are provided to the public.

This paper is an extended version of our previous conference paper published in the 25th Annual Conference on Neural Information Processing Systems (NIPS) 2011 [1].

1 Introduction

Even today, cell tracking remains a challenging topic that is under active study [2, 3], particularly in the context of high-content screening [4] and cell lineage reconstruction [5–7]. However, manual cell tracking is still predominant in practice [8] and life science researchers need tools that are accurate, configurable and yet require limited manual input [9]. Unlike tracking people or cars in videos [10], cellular image sequences usually contain large numbers (up to thousands) of objects which may be densely packed and be indiscernible by appearance (Fig. 1E). Also, due to physical or experimental limits, the temporal resolution may be so low that cells appear to be "jumping" between frames, showing rare spatial overlap (Fig. 1A). In addition, the underlying cellular activities may be diverse, including cell division (Fig. 1C&D), cell death, large deformation (Fig. 1B), leaving/entering the field of view, etc. Taken together, the estimation of inter-frame correspondences of cells becomes a very difficult task. Last but not least, the final result of a tracking-by-assignment depends on the previous cell segmentation/detection step. Despite many encouraging advances [11–13], segmentation/detection errors are inevitable and will propagate to tracking errors. This can cause misinterpretation, e.g. an over-segmentation can easily be mistaken for a cell division (Fig. 1F).

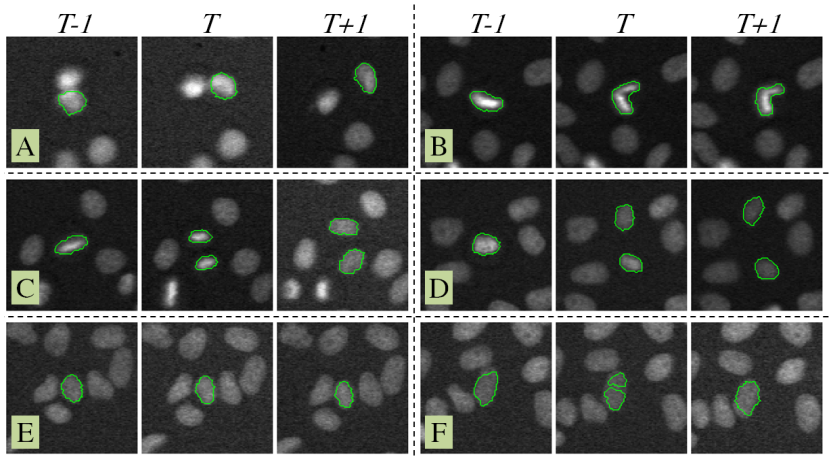

Figure 1: Challenges in cell tracking: A – relatively large displacement; B – large deformation; C&D – heterogeneous cell division appearance; E – dense and touching cells; F – segmentation error (over-segmentation). Three consecutive frames are shown and the boundary of the cells of interest are highlighted.

1.1 Taxonomy of Cell Tracking Methods

Existing cell tracking methods can broadly be categorized as deformable models, stochastic filtering and object assignment. Deformable models combine

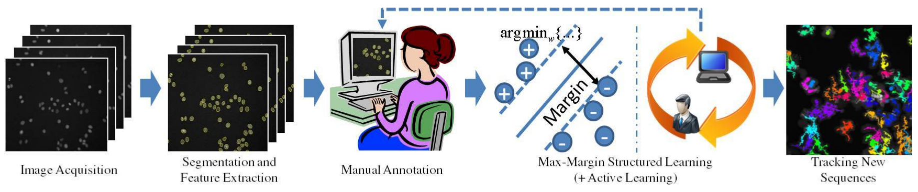
argmin$_w${...}
Margin
Image Acquisition
Segmentation and Feature Extraction
Manual Annotation
Max-Margin Structured Learning (+Active Learning)
Tracking New Sequences

Figure 2: Overview of our learning based approach. After some segmentation and tracking feature extraction, we take user's track annotation to train a cell tracking model. Active learning is also integrated to reduce the annotation effort. The trained model is then applied to new sequences.

detection, segmentation and tracking by initializing a set of models (e.g. active contours) in the first frame and updating them in subsequent frames [14–16]. Large displacements are difficult to capture with this class of techniques and are better handled by state space models, e.g. in the guise of stochastic filtering. The latter also allows for sophisticated observation models [17]. Stochastic filtering builds on a solid statistical foundation, but is often limited in practice due to its high computational demands. Object assignment methods make it harder to represent object properties, but they scale well [3,18,19], allowing the tracking of thousands of cells in 3D [20]. For the remainder of this paper, we concentrate on object assignment, or tracking-by-assignment, methods.

1.2 Machine Learning for Object Tracking

All of the above approaches contain energy terms whose parameters may be tedious or difficult to adjust. Recently, great efforts have been made to develop better energy terms with the help of machine learning techniques, mostly in the context of pedestrian tracking and traffic monitoring. Specifically, for tracking-by-assignment, this was first accomplished by casting tracking as a local affinity prediction problem with either offline [21] or online learning [22–24], weakly supervised learning with imperfect oracles [25], manifold appearance model learning [26], or ranking [27, 28]. However, these local methods fail to capture the very important dependency among assignments, hence the resulting local affinities do not necessarily guarantee a better global assignment [29]. To address this limitation, [30] extended the RankBoost method from [28] to rank global assignments represented as a Conditional Random Field (CRF). To reduce the annotation cost, active learning was also applied, e.g. in the context of video data labeling [31].

1.3 Advantages of Learning Based Tracking

We believe that a learning based approach has the following advantages over approaches without learning. Firstly, learning allows users to inject their prior knowledge in a form or language that is natural to them, namely direct cell-to-cell assignments between frames. This is more intuitive than specifying numerical values for parameters whose meaning, or effect, may remain obscure (as in parametric tracking approaches). Secondly, with learning, adding more annotations allows for systematical improvement of the model. Finally, it enables the use of very high-dimensional features. Though conventional grid parameter search is effective for models with low-dimensional features, it becomes inapplicable for high-dimensional ones for being too expensive (exponentially many combinations) and suboptimal (discretization of the parameter space).

1.4 Our Contributions

In comparison to previous cell tracking systems, our method is special in that it builds on the concept of learning from user annotated tracks. Our major contributions are as follows. We first present an extended formulation of the object assignment models that takes many complex tracking features and events into account. This generalization improves the expressiveness of the model, but also increases the number of parameters. We hence, secondly, propose to use max-margin structured learning to automatically learn optimum parameters from a training set, and hence profit fully from this richer description. Thirdly, to reduce the high cost of ground truth annotation, we further developed an active learning approach for efficient training data retrieval. To the best of our knowledge, this is the first active learning method for cell tracking. Finally, we share our considerations for a cell tracking framework and its usability, including design of tracking features, a novel visualization technique for annotation and validation, and a C++/Matlab software toolbox for the community.

1.5 Paper Organization

The rest of the paper is organized as follows. In section 2, we present the technical details of our tracking model and the learning algorithms (max-margin and active). We then share our considerations for feature design, visualization and software packages in section 3, followed by results in section 4. Finally, discussion and conclusions are provided in section 5 and section 6, respectively.

2 Algorithms

2.1 Tracking Model: Events, Hypotheses and Scoring

We assume that a previous detection and segmentation step has identified object candidates in all frames, see Fig. 2. We set out to find that set of object assignments that best explains these observations. To this end, we admit the following set $\boldsymbol{E}$ of standard events [3, 18]: a cell can *move* or *divide* and it can *appear* or *disappear*. In addition, we allow two cells to (seemingly) *merge*, to account for occlusion or under-segmentation; and a cell can (seemingly) *split*, to allow for the lifting of occlusions, or for over-segmentation. These additional hypotheses are useful to account for the errors that typically occur in the detection and segmentation step in crowded or noisy data. The distinction between division and split is reasonable given that typical fluorescence stains endow the anaphase with a distinctive appearance.

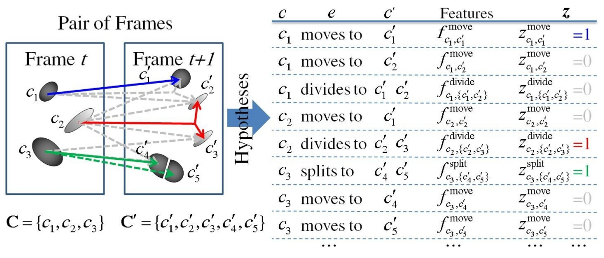

c	e	c'	Features	z	
c_1	moves to	c'_1	$f^{\text{move}}_{c_1,c'_1}$	$z^{\text{move}}_{c_1,c'_1}$	$=1$
c_1	moves to	c'_2	$f^{\text{move}}_{c_1,c'_2}$	$z^{\text{move}}_{c_1,c'_2}$	$=0$
c_1	divides to	c'_1 c'_2	$f^{\text{divide}}_{c_1,\{c'_1,c'_2\}}$	$z^{\text{divide}}_{c_1,\{c'_1,c'_2\}}$	$=0$
c_2	moves to	c'_1	$f^{\text{move}}_{c_2,c'_2}$	$z^{\text{move}}_{c_2,c'_2}$	$=0$
c_2	divides to	c'_2 c'_3	$f^{\text{divide}}_{c_2,\{c'_2,c'_3\}}$	$z^{\text{divide}}_{c_2,\{c'_2,c'_3\}}$	$=1$
c_3	splits to	c'_4 c'_5	$f^{\text{split}}_{c_3,\{c'_4,c'_5\}}$	$z^{\text{split}}_{c_3,\{c'_4,c'_5\}}$	$=1$
c_3	moves to	c'_4	$f^{\text{move}}_{c_3,c'_4}$	$z^{\text{move}}_{c_3,c'_4}$	$=0$
c_3	moves to	c'_5	$f^{\text{move}}_{c_3,c'_5}$	$z^{\text{move}}_{c_3,c'_5}$	$=0$
	…		…	…	…

Figure 3: Toy example: two sets of object candidates, and a small subset of the possible assignment hypotheses. One particular interpretation of the scene is indicated by colored arrows (left) or equivalently by a configuration of binary indicator variables $\boldsymbol{z}$ (rightmost column in table). Some rejected hypotheses are shown in gray (best viewed in color).

Table 1: Notations for Tracking Model

Notation	Definition
$\boldsymbol{x}$	Input data, detected objects from a pair of subsequent frames
$\boldsymbol{C}, \boldsymbol{C}'$	Set of objects from the first/second frame
$\mathcal{P}(\boldsymbol{C})$	$\mathcal{P}(\boldsymbol{C}) := \boldsymbol{C} \cup (\boldsymbol{C} \otimes \boldsymbol{C})$, union of $\boldsymbol{C}$ and all ordered pairs of objects in $\boldsymbol{C}$
$\boldsymbol{E}$	Set of all possible events
$\boldsymbol{z}$	Tracking result, assignments of objects
$\boldsymbol{f}^e_{c,c'}$	Feature vector for the assignment of $c \in \mathcal{P}(\boldsymbol{C})$ and $c' \in \mathcal{P}(\boldsymbol{C}')$ as event e
$\boldsymbol{w}^e$	Parameter vector for event e
$z^e_{c,c'}$	Binary indicator variable for the assignment of $c \in \mathcal{P}(\boldsymbol{C})$ and $c' \in \mathcal{P}(\boldsymbol{C}')$ as event e

We first define important notations in Table 1. Given sets of detected objects $\{\boldsymbol{C}, \boldsymbol{C}'\}$ from two subsequent frames, there is a multitude of possible assignment hypotheses, see Fig. 3. We have two tasks: firstly, to allow only consistent assignments (e.g. making sure that each cell in the second frame is accounted for only once); and secondly to identify, among the multitude of consistent hypotheses, the one that is most compatible with the observations, and with what we have learned from the training data.

We express this compatibility of the assignment between $c \in \mathcal{P}(\boldsymbol{C})$ and $c' \in \mathcal{P}(\boldsymbol{C}')$ by event $e \in \boldsymbol{E}$ as an inner product $\langle \boldsymbol{f}^e_{c,c'}, \boldsymbol{w}^e \rangle$. Here, $\boldsymbol{f}^e_{c,c'}$ is a feature vector that characterizes the discrepancy (if any) between object candidates c and c'; and $\boldsymbol{w}^e$ is a parameter vector that encodes everything we have learned from the training data. Summing over all object candidates in either of the frames and over all types of events gives the following compatibility function:

$$\mathcal{L}(\boldsymbol{x}, \boldsymbol{z}; \boldsymbol{w}) := \sum_{e \in \boldsymbol{E}} \sum_{c \in \mathcal{P}(\boldsymbol{C})} \sum_{c' \in \mathcal{P}(\boldsymbol{C}')} \langle \boldsymbol{f}^{e}_{c,c'}, \boldsymbol{w}^{e} \rangle z^{e}_{c,c'}, \tag{1}$$

where $\boldsymbol{z} = \left\{ z^{e}_{c,c'} \right\}$ is a set of binary variables whose element indicates whether a hypothesis is accepted. The compatibility function $\mathcal{L}(\boldsymbol{x}, \boldsymbol{z}; \boldsymbol{w})$ states how well a set of accepted hypotheses $\boldsymbol{z}$ matches the observations $\boldsymbol{f}(\boldsymbol{x})$ computed from the raw data $\boldsymbol{x}$, given the knowledge $\boldsymbol{w}$ from the training set.

Eq. (1) is equivalent to:

$$\mathcal{L}(\boldsymbol{x}, \boldsymbol{z}; \boldsymbol{w}) := \boldsymbol{w}' \Phi(\boldsymbol{x}, \boldsymbol{z}), \tag{2}$$

where $\boldsymbol{w}$ is the concatenation of event-specific parameter $(\boldsymbol{w}^{\text{move}}, \boldsymbol{w}^{\text{divide}}, \ldots)$ and $\Phi(\boldsymbol{x}, \boldsymbol{z})$ is the concatenation of event-specific features summed up over all activated events, which is referred to as joint feature vector [32]:

$$\Phi(\boldsymbol{x}, \boldsymbol{z}) = \begin{bmatrix} \sum_{c \in \mathcal{P}(\boldsymbol{C})} \sum_{c' \in \mathcal{P}(\boldsymbol{C}')} \boldsymbol{f}^{\text{move}}_{c,c'} z^{\text{move}}_{c,c'} \\ \sum_{c \in \mathcal{P}(\boldsymbol{C})} \sum_{c' \in \mathcal{P}(\boldsymbol{C}')} \boldsymbol{f}^{\text{divide}}_{c,c'} z^{\text{divide}}_{c,c'} \\ \\ \ldots \end{bmatrix} \tag{3}$$

Furthermore, the selection of $\boldsymbol{z}$ is subject to consistency requirements: each candidate in the first frame must have a single fate, and each candidate from the second frame a unique past. That is, for hypotheses associated with the same candidate, only one of them can be accepted. Formally, we have $\boldsymbol{z} \in \mathcal{Z}$, a space that satisfies the following constraints:

$$\forall c' \in \mathcal{P}(\boldsymbol{C}'), \sum_{e \in \boldsymbol{E}} \sum_{c \in \mathcal{P}(\boldsymbol{C})} z^{e}_{c,c'} = 1, \text{ (consistency)} \tag{4}$$

$$\forall c \in \mathcal{P}(\boldsymbol{C}), \sum_{e \in \boldsymbol{E}} \sum_{c' \in \mathcal{P}(\boldsymbol{C}')} z^{e}_{c,c'} = 1, \text{ (consistency)} \tag{5}$$

$$\forall e \in \boldsymbol{E}, c \in \mathcal{P}(\boldsymbol{C}), c' \in \mathcal{P}(\boldsymbol{C}'), z^{e}_{c,c'} \in \{0, 1\}. \text{ (booleanity)}$$

As an important technical detail, note that $\mathcal{P}(\boldsymbol{C}) := \boldsymbol{C} \cup (\boldsymbol{C} \otimes \boldsymbol{C})$ is a set comprising each object candidate, as well as all ordered pairs of object candidates from a frame. For the example in Fig. 3, $\mathcal{P}(\boldsymbol{C}) = \{c_1, c_2, c_3, \{c_1, c_2\}, \{c_1, c_3\}, \{c_2, c_3\}\}$. This allows us to conveniently subsume cell divisions, splits and mergers in the above equation.

To this end, model inference refers to finding the best $\boldsymbol{z} \in \mathcal{Z}$ that *maximizes* the compatibility function $\mathcal{L}(\boldsymbol{x}, \boldsymbol{z}; \boldsymbol{w})$:

$$\hat{\boldsymbol{z}} = \arg\max_{\boldsymbol{z} \in \mathcal{Z}} \mathcal{L}(\boldsymbol{x}, \boldsymbol{z}; \boldsymbol{w}). \tag{6}$$

The remaining tasks, discussed next, are how to learn the parameters $\boldsymbol{w}$ from the training data; given these, how to find the best possible $\boldsymbol{z}$; and finding useful features.

2.2 Structured Max-Margin Parameter Learning

2.2.1 Learning to Track by Risk Minimization

In learning the parameters automatically from a training set, we pursue two goals: first, to go beyond manual parameter tweaking in obtaining the best possible performance; and second, to make the process as facile as possible for the user. This is under the assumption that most experimentalists find it easier to specify what a correct tracking should look like, rather than what value a more-or-less obscure parameter should have.

Table 2: Notations for Learning

Notation	Definition
$\boldsymbol{X}$	Set of training data
$\boldsymbol{Z}^*$	Set of ground truth tracking annotations
$\lambda, \Omega(\boldsymbol{w})$	Regularization strength and regularization function
ξ_n	Slack variable for sample n
$\mathcal{Z}_n$	Space of all possible tracking solutions (structured) for sample n

Given N training frame pairs $\boldsymbol{X} = \{\boldsymbol{x}_n\}$ and their correct assignments $\boldsymbol{Z}^* = \{\boldsymbol{z}_n^*\}$, $n = 1, \ldots, N$, the best set of parameters is the optimizer of

$$\arg\min_{\boldsymbol{w}} \mathcal{R}(\boldsymbol{w}; \boldsymbol{X}, \boldsymbol{Z}^*) + \lambda\Omega(\boldsymbol{w}). \tag{7}$$

Here, $\mathcal{R}(\boldsymbol{w}; \boldsymbol{X}, \boldsymbol{Z}^*)$ measures the empirical loss of the current parametrization $\boldsymbol{w}$ given the training data $\boldsymbol{X}, \boldsymbol{Z}^*$. To prevent overfitting to the training data, this is complemented by the regularizer $\Omega(\boldsymbol{w})$ that favors parsimonious models. We use L_1 or L_2 regularization ($\Omega(\boldsymbol{w}) = ||\boldsymbol{w}||_p^p/p$, $p = \{1, 2\}$), i.e. a measure of the length of the parameter vector $\boldsymbol{w}$. The L_2 norm is often used for its numerical efficiency, while the L_1 norm is popular thanks to its potential to induce sparse solutions (i.e., some parameters can become zero). The empirical loss is given by $\mathcal{R}(\boldsymbol{w}; \boldsymbol{X}, \boldsymbol{Z}^*) = \frac{1}{N}\sum_{i=1}^N \Delta(\boldsymbol{z}_n^*, \hat{\boldsymbol{z}}_n(\boldsymbol{w}; \boldsymbol{x}_n))$. Here $\Delta(\boldsymbol{z}^*, \hat{\boldsymbol{z}})$ is a loss function that measures the discrepancy between a true assignment $\boldsymbol{z}^*$ and a prediction by specifying the fraction of missed events w.r.t. the ground truth:

$$\Delta(\boldsymbol{z}^*, \hat{\boldsymbol{z}}) = \frac{1}{|\boldsymbol{z}^*|} \sum_{e \in \boldsymbol{E}} \sum_{c \in \mathcal{P}(\boldsymbol{C})} \sum_{c' \in \mathcal{P}(\boldsymbol{C}')} z_{c,c'}^{*e}(1 - \hat{z}_{c,c'}^{e}). \tag{8}$$

This decomposable function allows for easy exact inference when solving Eq. (9) [33]. Note that this loss only penalizes false negatives. We do not explicitly penalize false positives, because they are already interconnected through the consistency constraints in Eq. (4) and Eq. (5).

2.2.2 Max-Margin Structured Learning

Importantly, note that under constraints Eq. (4) and Eq. (5) both the input (objects from a pair of frames) and output (assignments between objects) in this learning problem are *structured* – a set of variables that are interdependent. We hence resort to max-margin structured learning [32] to exploit the structure and dependency within the assignment hypotheses. In comparison to other aforementioned learning methods, structured learning allows us to directly learn the global affinity measure, avoid generating many artificial false assignment samples, and drop any assumptions on the signs of the features. Structured learning has been successfully applied to many complex real world problems such as word/sequence alignment, graph matching, and image segmentation [34].

In particular, we attempt to find the decision boundary that maximizes the margin between the correct assignment $\boldsymbol{z}_n^*$ and the closest runner-up solution. An equivalent formulation is the condition that the score of $\boldsymbol{z}_n^*$ be greater than that of any other solution by some margin. To prevent overfitting, one can relax this constraint by introducing slack variables ξ_n, which finally yields the following objective function for the max-margin structured learning problem from Eq. (7):

$$\begin{array}{ll} \underset{\boldsymbol{w},\boldsymbol{\xi}\geq\boldsymbol{0}}{\arg\min} & \frac{1}{N}\sum_{n=1}^{N}\xi_n + \lambda\Omega(\boldsymbol{w}) \\ \text{s. t.} & \forall n, \forall \hat{\boldsymbol{z}}_n \in \mathcal{Z}_n : \\ & \mathcal{L}(\boldsymbol{x}_n, \boldsymbol{z}_n^*; \boldsymbol{w}) - \mathcal{L}(\boldsymbol{x}_n, \hat{\boldsymbol{z}}_n; \boldsymbol{w}) \geq \Delta(\boldsymbol{z}_n^*, \hat{\boldsymbol{z}}_n) - \xi_n, \end{array} \tag{9}$$

where $\mathcal{Z}_n$ is the set of possible consistent assignments and using $\Delta(\boldsymbol{z}_n^*, \hat{\boldsymbol{z}}_n)$ instead of a fixed margin is known as "margin-rescaling" [32]. Intuitively, it pushes the decision boundary further away from the "bad" solutions with high losses. Note that the loss in Eq. (9) is $\xi_n = |\Delta(\boldsymbol{z}_n^*, \hat{\boldsymbol{z}}_n) - \mathcal{L}(\boldsymbol{x}_n, \boldsymbol{z}_n^*; \boldsymbol{w}) + \mathcal{L}(\boldsymbol{x}_n, \hat{\boldsymbol{z}}_n; \boldsymbol{w})|_+$, which is a tight, convex upper bound on the original loss in Eq. (7) (non-convex).

2.2.3 Optimization with Bundle Method

Since Eq. (9) involves an exponential number of constraints, the learning problem cannot be represented explicitly, let alone solved directly. We thus resort to the *bundle method* [35] which, in turn, is based on the *cutting-planes* approach [32]. The basic idea is as follows. Start with some parametrization $\boldsymbol{w}$ and no constraints. At iteration t, first find the optimum assignments for the current $\boldsymbol{w}$ by solving, for all n,

$$\hat{\boldsymbol{z}}_n = \arg\max_{\boldsymbol{z}\in\mathcal{Z}_n}\{\mathcal{L}(\boldsymbol{x}_n, \boldsymbol{z}; \boldsymbol{w}) + \Delta(\boldsymbol{z}_n^*, \boldsymbol{z})\}. \tag{10}$$

Use all $\hat{\boldsymbol{z}}_n$ to identify the most violated constraint, which is a linear lower bound of the average of the slack variables [35]:

$$\boldsymbol{a}_t'\boldsymbol{w} + b_t \leq \frac{1}{N}\sum_{n=1}^{N}\xi_n, \tag{11}$$

where, given $\Psi(\boldsymbol{x}, \boldsymbol{z}^*, \hat{\boldsymbol{z}}) := \Phi(\boldsymbol{x}, \boldsymbol{z}^*) - \Phi(\boldsymbol{x}, \hat{\boldsymbol{z}})$, we have

$$\boldsymbol{a}_t = -\frac{1}{N}\left(\sum_n^N \Psi(\boldsymbol{x}_n, \boldsymbol{z}_n^*, \hat{\boldsymbol{z}}_n)\right), \tag{12}$$

$$b_t = -\frac{1}{N}\left[\sum_{n=1}^N \Delta(\boldsymbol{z}_n^*, \hat{\boldsymbol{z}}_n) + \boldsymbol{w}'\Psi(\boldsymbol{x}_n, \boldsymbol{z}_n^*, \hat{\boldsymbol{z}}_n)\right] - \boldsymbol{w}'\boldsymbol{a}_t. \tag{13}$$

We then update $\boldsymbol{w}$ by solving a variant of Eq. (9), which instead uses all those most-violated constraints (incl. those from previous iterations)

$$\begin{aligned} \underset{\boldsymbol{w},\boldsymbol{\xi}\geq\mathbf{0}}{\arg\min} \quad & \frac{1}{N}\sum_{n=1}^N \xi_n + \lambda\Omega(\boldsymbol{w}) \\ \text{s. t.} \quad & \forall i \in \{1,\ldots,t\}, \boldsymbol{a}_i'w + b_i \leq \frac{1}{N}\sum_n^N \xi_n. \end{aligned} \tag{14}$$

We then move on to the next iteration: find new best assignments using the updated $\boldsymbol{w}$, etc. The procedure converges when those constraints form a tight lower bound of the original objective function (Eq. (7)), which is measured by so-called approximation gap ϵ (see [35] for more details). For a given parameter $\boldsymbol{w}$, the optimum assignments can be found by integer linear programming (ILP) [3,18,19].

Pseudocode is shown in Fig. 4.

```
 1: Input: $\boldsymbol{D} = \{(\boldsymbol{x}_n, \boldsymbol{z}_n^*)\}_{n=1}^N, \hat{\epsilon}$
 2: Initialize $\boldsymbol{A} = \emptyset, \boldsymbol{b} = \emptyset, t = 1$, $\boldsymbol{w}$ (randomly)
 3: repeat
 4:     for all $(\boldsymbol{x}, \boldsymbol{z}^*) \in \boldsymbol{D}$ do
 5:         Compute $\hat{\boldsymbol{z}}$ using Eq. 10
 6:     end for
 7:     Compute $\boldsymbol{a}_t$ and $b_t$ as in Eq. 12 and Eq. 13
 8:     Set $\boldsymbol{A} = \boldsymbol{A} \cup \boldsymbol{a}_t$ and $\boldsymbol{b} = \boldsymbol{b} \cup b_t$
 9:     Update $\boldsymbol{w}$ with $\boldsymbol{A} = \{\boldsymbol{a}_1, \ldots\}$, $\boldsymbol{b} = \{b_1, \ldots\}$ (Eq. 14)
10:     Compute approximation gap $\epsilon$
11:     Set $t = t + 1$
12: until $\epsilon \leq \hat{\epsilon}$
13: Output: $\boldsymbol{w}$
```

Figure 4: Max-margin structured learning.

2.3 Training Data Retrieval via Active Learning

Given a learning algorithm, training a highly predictive tracking model is still dependent on the amount and quality of annotated training samples. Unfortunately, the annotation effort is particularly high for our tracking problem –

hundreds of cells have to be examined and hundreds of events have to be marked per training sample (a pair of images). Therefore, we introduce an active learning approach for efficient training data retrieval at a low annotation cost. Our approach has the following core components: patchification, uncertainty measure, model update and stopping criteria. We elaborate on the details following the pseudocode shown in Fig. 5.

```
1: Input: $\boldsymbol{D} = \{\boldsymbol{x}_n\}_{n=1}^{N}, \hat{\eta}, T$
2: Initialize $\boldsymbol{D}_\mathrm{L} = \emptyset, \boldsymbol{D}_\mathrm{U} = \boldsymbol{D}, t = 1$, $\boldsymbol{w}$ (randomly)
3: repeat
4:    Find $\tilde{\boldsymbol{x}} = \arg\max_{\boldsymbol{x} \in \boldsymbol{D}_\mathrm{U}} q(\boldsymbol{x}, \boldsymbol{w})$
5:    Annotate $\tilde{\boldsymbol{z}}^*$
6:    Set $\boldsymbol{D}_\mathrm{U} = \boldsymbol{D}_\mathrm{U} \setminus \tilde{\boldsymbol{x}}$
7:    Set $\boldsymbol{D}_\mathrm{L} = \boldsymbol{D}_\mathrm{L} \cup \{(\tilde{\boldsymbol{x}}, \tilde{\boldsymbol{z}})\}$
8:    for all $(\boldsymbol{x}, \boldsymbol{z}^*) \in \boldsymbol{D}_\mathrm{L}$ do
9:       Compute $\hat{\boldsymbol{z}}$ using Eq. 10
10:      Update $\boldsymbol{w} = \boldsymbol{w} + \Phi(\boldsymbol{x}, \boldsymbol{z}^*) - \Phi(\boldsymbol{x}, \hat{\boldsymbol{z}})$
11:   end for
12:   Compute average uncertainty $\bar{q}_t = \frac{1}{|\boldsymbol{D}_\mathrm{U}|} \sum_{\boldsymbol{x} \in \boldsymbol{D}_\mathrm{U}} q(\boldsymbol{x}, \boldsymbol{w})$
13:   Compute convergence measure $\eta(\bar{q}_{t-T:t})$ (Eq. 16)
14:   Set $t = t + 1$
15: until $\eta(\bar{q}_{t-T:t}) \leq \hat{\eta}$ or $\boldsymbol{D}_\mathrm{U} \equiv \emptyset$
16: Output: $\boldsymbol{w}$
```

Figure 5: Active structured learning with perceptron.

1) Patchification refers to dividing a pair of full images (large, hundreds of events) into pairs of local patches (small, normally less than 20 cells per frame with patch size 128×128). Then each pair of local patches is considered a training sample. This certainly breaks the original (large) structure of event dependency induced by Eq. (4) and Eq. (5). Yet, we will empirically show that training on patchified samples is just as effective as training on pairs of full images. We consider patchification a necessary and viable pre-processing step for active learning. Otherwise, annotating a single sample is already too tedious and time-consuming, and part of the efforts is wasted on similar and repeated event patterns.

Note that patchification induces lots of artificial appearances and disappearances at the patch border. We eliminate them by discarding objects that touch the patch border unless it is the true image border.

2) Uncertainty measure is the very core component of active learning [36]. We propose four different uncertainty measures described in Table 3. They are direct extensions of uncertainty measures for flat data [37,38] to structured data as in this paper. As lines 4–6 of Fig. 5 shows, at each iteration, we find the most uncertain sample (viz. pair of patches) from all unlabeled samples $\boldsymbol{D}_\mathrm{U}$ and demand annotation from the annotator. We will compare the learning curves of those uncertainty measures in results.

Table 3: List of uncertainty sampling strategy.

Name	$q(\boldsymbol{x}, \boldsymbol{w})$ Formulation and Description
Random	Random number between 0 and 1
Scoring	$\exp\left(-\max\limits_{\boldsymbol{z}\in\boldsymbol{\mathcal{Z}}} \boldsymbol{w}'\Phi(\boldsymbol{x},\boldsymbol{z})\right)$ where higher value of $\max\limits_{\boldsymbol{z}\in\boldsymbol{\mathcal{Z}}} \boldsymbol{w}'\Phi(\boldsymbol{x},\boldsymbol{z})$ indicates higher confidence on the predicted tracking using existing parameter $\boldsymbol{w}$.
Best Vs. Worst	$\exp\left(-\left(\max\limits_{\boldsymbol{z}\in\boldsymbol{\mathcal{Z}}} \boldsymbol{w}'\Phi(\boldsymbol{x},\boldsymbol{z}) - \min\limits_{\boldsymbol{z}\in\boldsymbol{\mathcal{Z}}} \boldsymbol{w}'\Phi(\boldsymbol{x},\boldsymbol{z})\right)\right)$ where larger margin between those two terms indicates higher confidence towards the best predicted tracking w.r.t the worst one.
Best Vs. 2nd	$\exp\left(-\left(\max\limits_{\boldsymbol{z}\in\boldsymbol{\mathcal{Z}}} \boldsymbol{w}'\Phi(\boldsymbol{x},\boldsymbol{z}) - \max\limits_{\boldsymbol{z}\in\boldsymbol{\mathcal{Z}}^\circ} \boldsymbol{w}'\Phi(\boldsymbol{x},\boldsymbol{z})\right)\right)$ where $\max_{\boldsymbol{z}\in\boldsymbol{\mathcal{Z}}^\circ} \boldsymbol{w}'\Phi(\boldsymbol{x},\boldsymbol{z})$ means computing the second best scoring and larger margin between those two terms indicates higher confidence towards the best predicted tracking w.r.t the second best one.

As technical details, to compute the worst predicted tracking with given $\boldsymbol{w}$ (see *Best vs. Worst*, Table 3), we can simply flip the signs of $\boldsymbol{w}$ and call Eq. (6). Computing the second best tracking (see *Best vs. 2nd*, Table 3) is a bit more complicated. Briefly, we first compute the best tracking $\hat{\boldsymbol{z}}$ using Eq. (6). Then the second best tracking $\hat{\hat{\boldsymbol{z}}}$ can be computed by Eq. (15) which is a variant of Eq. (6) with one extra constraint. The rational is as follows: $2\hat{\boldsymbol{z}}-1$ transforms all the 0s in the binary vector $\hat{\boldsymbol{z}}$ to -1s, so the maximum possible value of $\langle 2\hat{\boldsymbol{z}}-1, \boldsymbol{z}\rangle$ is $\|\hat{\boldsymbol{z}}\|_1$ and is achieved only when $\boldsymbol{z} = \hat{\boldsymbol{z}}$; by forcing $\langle 2\hat{\boldsymbol{z}}-1, \boldsymbol{z}\rangle \le \|\hat{\boldsymbol{z}}\|_1 - 1$, the optimizer can never pick $\hat{\boldsymbol{z}}$ as the optimal solution.

$$\begin{aligned} \hat{\hat{\boldsymbol{z}}} = \quad & \arg\max\nolimits_{\boldsymbol{z}\in\mathcal{Z}} \quad \mathcal{L}(\boldsymbol{x}, \boldsymbol{z}; \boldsymbol{w}) \\ & \text{s. t.} \qquad \langle 2\hat{\boldsymbol{z}}-1, \boldsymbol{z}\rangle \le \|\hat{\boldsymbol{z}}\|_1 - 1. \end{aligned} \tag{15}$$

3) Model update refers to updating the model parameter $\boldsymbol{w}$ after receiving a new annotated sample. Given labeled training set ($\boldsymbol{D}_\text{L}$, Fig. 5), a naïve way is to invoke max-margin structured learning from the previous section (Eq. (9)). However, this turns out inefficient in practice: max-margin structured learning is known very expensive (see [32] and our runtime result), which means that the annotator has to wait a few minutes before proceeding to the next sample. Therefore, we resort to structured perceptron [39] for model update (lines 8–11, Fig. 5). Briefly, it makes a one-pass run through all labeled samples and updates the parameter by incrementally (and locally) adding the gradient, viz. $\boldsymbol{w} = \boldsymbol{w} + \partial_{\boldsymbol{w}} \left(\mathcal{L}(\boldsymbol{x}, \boldsymbol{z}^*; \boldsymbol{w}) - \mathcal{L}(\boldsymbol{x}, \hat{\boldsymbol{z}}; \boldsymbol{w})\right)$ (equivalent to line 10, Fig. 5).

Theorem 1 *Assuming a pool of N unannotated samples, the complexity of the proposed algorithm in Fig. 5 is $\mathcal{O}(N^2)$. While the complexity of using max-margin structured learning for model update is at least $\mathcal{O}(N^3)$.*

Proof: In Fig. 5, at each iteration t $(1 \leq t \leq N)$ we need N predictions, among which $N - t$ predictions are for uncertainty estimation on unlabeled samples (line 4) and the rest t for model update using labeled sampled (lines 8–11). This gives TN predictions after T iterations. Since T is a fraction of N, the overall complexity is $\mathcal{O}(N^2)$.

In the case of max-margin structured learning for model update (viz. replacing lines 8–11 with the algorithm in Fig. 4), [40] shows that, in SVM like max-margin formulation (incl. structured learning), the number of support vectors scales at least linearly with the number of training samples. Thus, the complexity of max-margin structured learning is at least quadratic because we need compute the inner-product of each support vector and each sample. The overall complexity is then at least $\sum_t \left[(N-t) + t^2\right]$, which amounts to $\mathcal{O}(N^3)$.

We will discuss other pros and cons in section 2.4.

4) Stopping criteria are another crucial component [36]. We chose a very popular measure proposed in [41] – the average uncertainty over all remaining unlabeled samples (see uncertainty measure in Table 3). This does not require any holdout validation dataset. At iteration t, given a sequence of computed average uncertainty $\bar{q}_{t-T:t}$ (incl. previous ones), we compute the convergence measure η using Eq. (16) [42] (lines 12–13, Fig. 5). This convergence measure drops to a low value when the improvement on average uncertainty remains minor for several iterations. We stop the active learning when the convergence measure is below a given threshold or all samples are labeled (line 15, Fig. 5).

$$\eta(\bar{q}_{1:T+1}) = |\widehat{\mathrm{mean}}(\bar{q}_{2:T+1}) - \widehat{\mathrm{mean}}(\bar{q}_{1:T})| \tag{16}$$

Here, $\widehat{\mathrm{mean}}(\cdot)$ is the robust mean (viz. mean of the elements within the 10% and 90% quantile).

2.4 A Combined Learning Strategy

Though gaining speed, using structured perceptron for model update has two drawbacks: lack of regularization and local (thus noisy) gradient update (line 10, Fig. 5). This makes the learned model prone to overfitting and also unstable in convergence (see results). Therefore, in practice we use a combined approach: we use active structured perceptron *only* for training data retrieval and then use max-margin structured learning to obtain a regularized and globally optimized model.

3 Framework and Usability

This section covers other important considerations for a cell tracking framework, including tracking features, visual editing tool and implementation/software.

3.1 Framework: Design of Tracking Features

The above structured learning for cell tracking allows the use of a much extended set of features to capture complicated events from different aspects, and thus boost the tracking performance. Many interesting tracking features have been proposed in previous work. We borrow some state-of-the-art [18, 19], and also contribute several new (e.g. Fig. 6). Table 4 shows a categorization of our tracking features. For a detailed list, please refer to the **supporting document**. Note that these features can vary significantly in scale, which makes manual parameter tuning difficult. Normalization helps, yet can not address the problem at its root. In the following, we briefly describe the features designed for different events.

Table 4: Categorization of features.

Type	Description
Position	difference in position, distance to border, overlap with border
Intensity	difference in intensity histogram/sum/mean/deviation, intensity of father cell
Shape	difference in shape, difference in size, shape compactness, shape evenness
Others	angle pattern, mass evenness, eccentricity of father cell

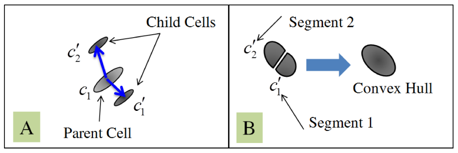

Figure 6: Illustration of features: A – angle pattern; B – shape compactness. Angle pattern measures whether the vectors pointing from the parent cell to the child cells form an angle close to 180°. Shape compactness is the ratio of the total area of two proximate segments (c'_1 and c'_2) divided by the area of the convex hull of their union.

3.2 Framework: Implementation and Software Contributions

Our framework has been implemented using Matlab and C++. The annotation GUI and active learning are written in Matlab for better interactivity, while the computation-intensive components such as feature extraction, model inference and max-margin structured learning are provided in C++. In practice, to reduce the search space and eliminate hypotheses with no prospect of being realized, we constrain the hypotheses to a k-nearest neighborhood (usually $k = 4$) with distance thresholding. We use IBM CPLEX[1] as the underlying optimization platform for the ILP and quadratic programming as needed for solving Eq. (9) [35]. In addition to those tracking features proposed in this paper, the core library also provides a generic interface for adding additional features using the factory design pattern. The library also allows for configurable settings for different applications (e.g. worm tracking, no division event). This enables users to easily integrate their preferred features. Our software library is available at

http://hci.iwr.uni-heidelberg.de/Staff/xlou/research/tracking.html.

3.3 Usability: Active Learning and Glyph Visualization

The improved usability first attributes to the use of active learning, which obtains the most informative sample to annotate. We further facilitate annotation by exploiting a visualization technique called "glyph visualization" [43] from the information visualization community [44]. Briefly, when two frames are placed side-by-side, instead of drawing arrows (e.g. Fig. 7A, cluttered view) or colored text (e.g. cell ID, more perception time), we draw two identical markers (viz. glyphs in the visualization language) at their respective cell centers to represent an assignment. We make the markers for proximate cells differ in several primitive attributes such as color and shape, which forms a local pattern. As a consequence, users no longer need to match cells by arrows or cell IDs but can use **local patterns** instead (viz. group by group in Fig. 7B, clean). This is efficient thanks to our powerful vision system: we instantly recognize and differentiate local patterns. Furthermore, incorrect tracking is easily discernible because of the consistency constraints (see Eq. (4) and Eq. (5)), namely a single error usually provokes a domino effect, leading to a strong perturbation of the glyph pattern. Important events such as divisions are still highlighted using arrows; however, being rare, they barely give rise to any visual clutter.

4 Results

We evaluated the proposed approach on five publicly available image sequences, one from DCellIQ[2] [19] and four from Mitocheck[3] [45] (referred to as MC1, MC2, ...). The datasets differ in illumination, cell density and image compression artifacts (Fig. 8 and Table 5). The imaging conditions for MC1 to MC4 are generally consistent, which differ from DCellIQ slightly. Note that re-training is necessary when applying the proposed approach to datasets with drastically different imaging conditions.

The GFP stained cell nuclei were segmented using the method in [13], yielding an F-score over 99.3% by counting. Some statistics about these two datasets

[1]www-01.ibm.com/software/integration/optimization/cplex-optimizer/

[2]www.cbi-tmhs.org/Dcelliq/files/051606_HeLaMCF10A_DMSO_1.rar

[3]www.mitocheck.org

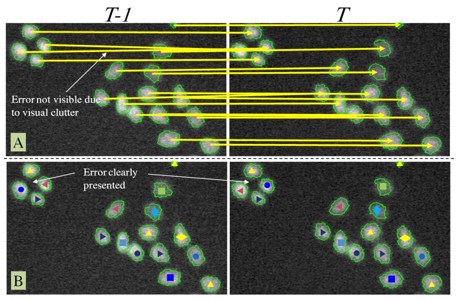

Figure 7: Comparison of line visualization and our glyph visualization as assignment indicator: A – line visualization, cluttered and errors not obvious; B – glyph visualization, tends to be cleaner and afford an easier overview.

are shown in Table 5. Note that our tracking approach is not restricted to the specific segmentation method used. Yet, high quality segmentation is expected since many tracking features are extracted using segmentation masks.

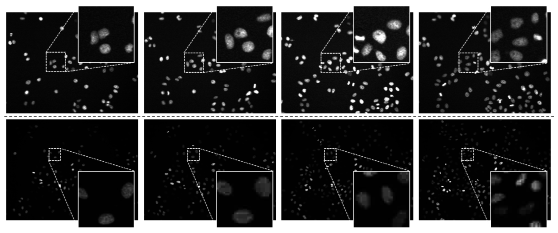

Figure 8: Selected raw images from DCellIQ (top) and MC4 (bottom). MC4 exhibits higher cell density, larger intensity variability and “blockness” artifacts due to image compression.

Table 5: Statistics of datasets used in our study

Data	Size ($X \times Y \times T$)	No. Cells	Seg. Acc.	Compressed
DCellIQ	$512 \times 672 \times 100$	10664	99.5%	No
MC1	$1024 \times 1344 \times 93$	37539	99.6%	No
MC2	$1024 \times 1344 \times 95$	19206	99.7%	No
MC3	$1024 \times 1344 \times 95$	12872	99.3%	No
MC4	$1024 \times 1344 \times 94$	24102	99.3%	Yes

4.1 Performance of Max-Margin Structured Learning

This section aims at evaluating max-margin structured learning. Therefore, we assume that sufficient annotation efforts can be provided. All results in this section are from models trained on full samples.

1) Task 1: Efficient Tracking for a Given Sequence

We first evaluate our method on a task that is frequently encountered in practice: the user simply wishes to obtain a good tracking for a given sequence with the smallest possible effort. The original graph matching based method on this sequence by [19] yields a loss of 6.18% (Table 6, 2nd row). The model in [18] using only two types of features (size and position) reduces this loss to 1.64% (Table 6, 1st row). A detailed analysis of the error counts for specific events shows that the method accounts well for moves, but has difficulty with disappearance and split events. This is mainly due to the limited descriptive power of the simple features used. To understand this limit, we applied our max-margin structured learning to optimize the model in [18] and obtained a reduction of the total loss from 1.64% to 0.65% (Table 6, 4th row). This can be considered as the limit of this model. Note that the learned parametrization actually deteriorates the detection of divisions because the learning aims at minimizing the overall loss across all events. Local learning [1] also has a reasonable result (Table 6, 3rd row).

Table 6: Performance comparison on the DCellIQ dataset. The header row shows the number of events occurring for moves, divisions, appearance, disappearance, splits and mergers. The remaining entries give the error counts for each event, summed over the entire sequence.

DCellIQ - Event	Moves	Divisions	Appear.	Disapp.	Splits	Mergers	Sum	Loss
Count	10156	104	78	76	54	55	10523	
[18] w/ suggested param.	71	18	16	26	30	12	173	1.64%
Original method [19]	-	-	-	-	-	-	-	6.18%[a]
Local learning by RF [1]	18	14	2	**0**	12	13	59	0.55%
[18] w/ our learning	21	25	5	5	6	10	72	0.65%
Ours w/ manual tweaking	56	24	16	19	2	**5**	122	1.12%
Ours w/ learning	**15**	**6**	**4**	1	**2**	6	**34**	**0.30%**

[a]Here we use the best reported error matching rate in [19] (similar to our loss).

Our model contains 38 features and thus manual tweaking becomes difficult (Table 6, 5th row). However, the proposed structured learning allows our model to fully profit from this richer description and achieve a total loss of only **0.30%** (Table 6, 6th row). More precisely, our model only missed **34** events which is much lower than the rest. Some example assignments are shown in Fig. 9.

The learned parameters are summarized in Fig. 10. They afford the following observations: Firstly, features on cell size and shape are generally of high importance, which is in line with the assumption in [18]. Secondly, the correlations of the features with the final assignment score are automatically learned. For example, shape compactness is positively correlated with split but negatively with division. This is in line with the intuition that an oversegmentation conserves compact shape, while a true division pushes the child cells far away from each other (in the present kind of data, where only DNA is labeled). Finally, many features are associated with large weights, which is key to the improved expressive power.

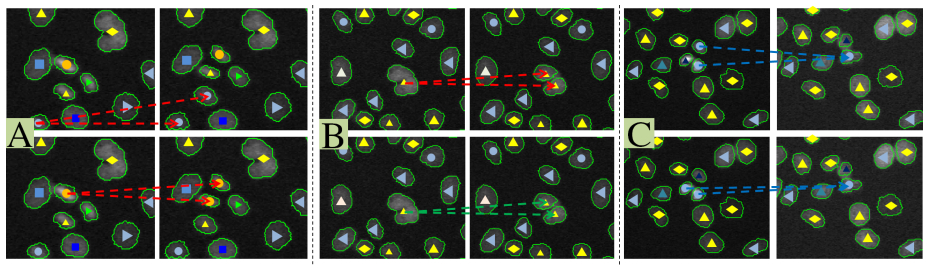

Figure 9: Some diverging assignments by [18] (top) and our approach (bottom): A – missing a false division event; B – split mistaken for division; C – false merger and move event. Color code: move – glyph visualization; red – division; green – split; blue – merger (best viewed in color).

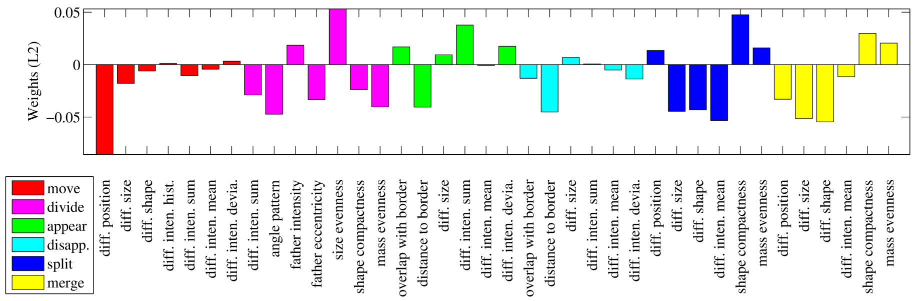

Figure 10: Parameters $\boldsymbol{w}$ learned from the training data. Parameters weighing the features for different events are colored differently. The parameter values indicate the correlations of the features with the respective event, i.e. the importance of each feature for the according event is measured by the absolute value of its weight parameter. Note that the correlation can be positive or negative.

2) Task 2: Tracking for High-Throughput Experiments

The experiment described in the foregoing draws both training and test samples from the same time lapse experiment. However, in high-throughput experiments such as in the Mitocheck project [45], it is more desirable to train on one or a few sequences, and make predictions on many others. To emulate this situation, we have used the parameters $\boldsymbol{w}$ trained in the foregoing on DCellIQ [19] and used these to track the Mitocheck dataset, without further training or refinement of the parameters. The main focus of the Mitocheck project is on accurate detection of mitosis (cell division). Despite the difference between those datasets, our method shows a high generalization capability and obtains an average total loss of $0.59\% \pm 0.33\%$, see Table 7. The relatively degraded performance on MC4 stems from the fact the video sequence is compressed which eventually yields noisy tracking features (e.g. blockness, intensity loss). Our method consistently outperforms [18] even if their parameters are optimized using our learning algorithm.

Table 7: Performance comparison on the Mitocheck datasets. The method was trained on the DCellIQ dataset. The header row shows the number of events occurring for moves, divisions, appearance, disappearance, splits and mergers. The remaining entries give the error counts for each event, summed over the entire sequence.

MC1 - Event	Moves	Divisions	Appear.	Disappear.	Splits	Mergers	Sum	Loss
Count	35845	465	363	335	174	217	37399	
[18] w/ our learning	50	66	30	36	109	63	354	1.04%
Ours w/ learning	30	23	30	30	56	30	199	0.56%
MC2 - Event	Moves	Divisions	Appear.	Disappear.	Splits	Mergers	Sum	Loss
Count	18957	195	59	99	90	78	19478	
[18] w/ our learning	17	69	7	3	43	10	149	0.82%
Ours w/ learning	10	10	7	3	17	10	57	0.24%
MC3 - Event	Moves	Divisions	Appear.	Disappear.	Splits	Mergers	Sum	Loss
Count	12493	118	105	78	109	102	13005	
[18] w/ our learning	13	40	7	13	69	20	162	1.13%
Ours w/ learning	7	20	7	10	23	13	80	0.56%
MC4 - Event	Moves	Divisions	Appear.	Disappear.	Splits	Mergers	Sum	Loss
Count	22520	384	310	304	127	132	23777	
[18] w/ our learning	102	92	49	35	79	21	378	1.44%
Ours w/ learning	109	22	57	33	48	9	278	1.03%

Fig. 11 shows the trajectories of lineages extracted from MC4. The background shows the maximum intensity projection through the image sequence. Each lineage is associated with a unique color – the root is indicated with a circle and all its descendants are colored the same. We see heterogeneous migrations and expansions, and cells are generally growing towards empty space in the field of view.

3) On Mitosis Event Detection: Specific vs. Conjunctive

Cell division, or mitosis, usually draws particularly high attention from life science researchers. Methods have been developed to specifically detect this event [45, 46]. We show that mitosis detection can be improved if it is considered in conjunction with other events, as is done in our approach. With appropriately learned features, we can significantly reduce ambiguity and eliminate false positives. For the DCellIQ sequence which is partially used for training, we successfully detected 98/104 events (see Table 6). For the more challenging MC4 dataset (for testing only), we correctly found 94.3% of 384 mitotic events.

4.2 Performance of Active Structured Learning

Knowing that we can train a highly predictive cell tracking model given sufficient training data, we now evaluate our active learning for annotation cost reduction.

1) Justification of Patchification: As a strong prerequisite for the success of active learning, we first need to justify patchification. We made a direct comparison by applying regularized max-margin training on full samples (pairs of full images) and on their respective patchified samples. Training samples are sampled from DCellIQ and the test data is MC4. After 10 repeated experiments,

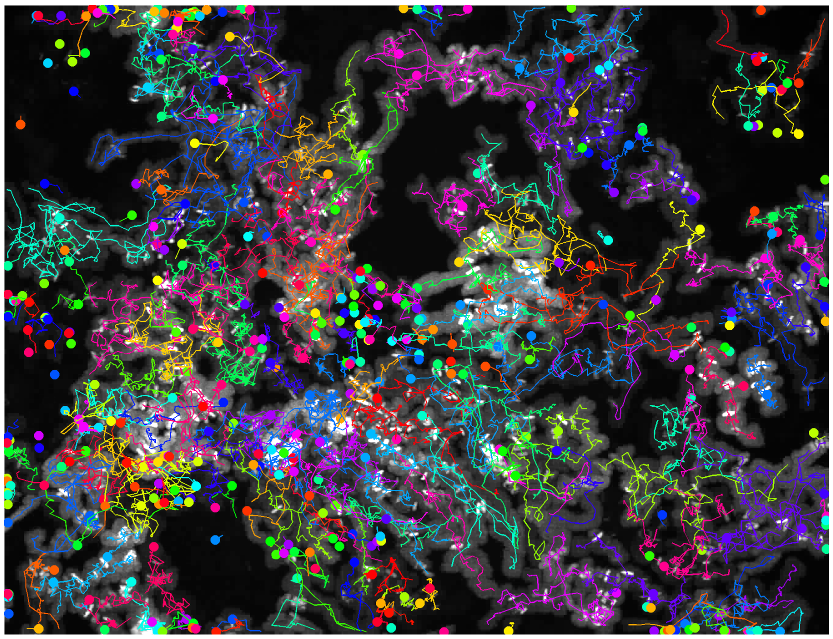
Figure 11: Trajectory of lineages (best viewed in color).

the test error for training with patchified samples is 1.10 ± 0.01 (unit: %), which is comparable to that of full samples: 1.08 ± 0.01 (unit: %). Note that patchification is only applied to training data and the test data is **not** patchified.

2) Uncertainty Measures and Stopping Criteria: Using 660 patchified training samples from the DCellIQ dataset, in Fig. 12 we compare the learning curves (viz. average uncertainty) of the four uncertainty measures upto 50% of the total training samples. *Best vs. Worst* is stably converging at the beginning but has a second wave of significant changes after 16% of total training samples. The same applies to *Scoring* but the changes of average uncertainty are more drastic. *Best vs. 2nd* appears to be the best performing one: it converges to a stable state after 17% of total training samples. Regarding stopping criteria, *Random* is excluded because it is not suitable for the uncertainty convergence measure η (Eq. (16)). To compute η, we chose $T = 80$ and used 10^{-4} as the stopping threshold. As the embedded figure in Fig. 12 shows, they all stop at around 17% of training data (*Best vs. Worst* is a bit earlier).

To further understand the learning curve in a practical setting, we tested all intermediate learned parameter $\boldsymbol{w}$ of the active learning process on MC4, respectively for all uncertainty measures. The result in Fig. 13 further supports our choice of *Best 2nd* not only because of its superiority in stability but also for its lower test error. Note that this observation is in line with the principle of max-margin.

The second wave in the learning curve of *Scoring* and *Best vs. Worst* sug-

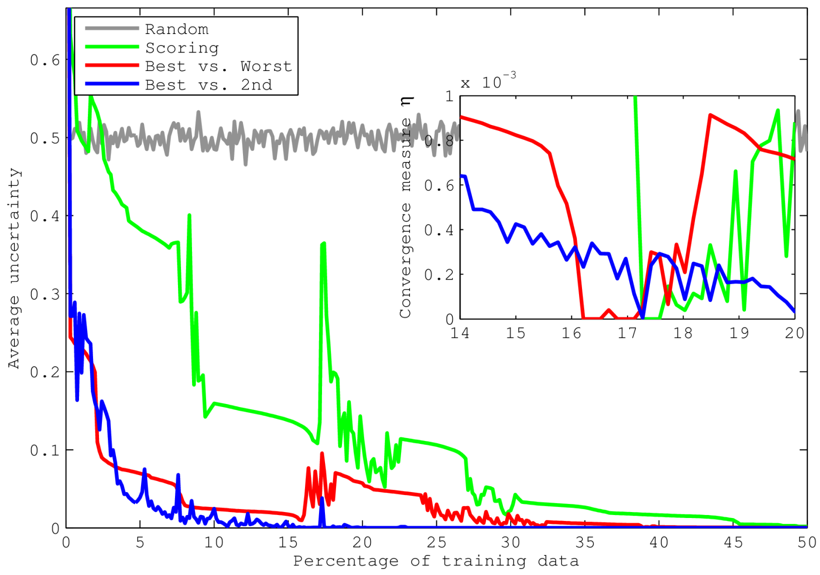

Figure 12: Comparison of uncertainty measures: average uncertainty vs. percentage of training data. The embedded figure shows the uncertainty convergence η vs. the percentage of training data.

gests that there are two principle cohorts in the training datasets. Both *Scoring* and *Best vs. Worst* get stuck in choosing samples mostly from one cohort and consequently make the trained model overfit to this cohort. This is recognized only when the overfitting is too severe and the second cohort becomes dominant in the remaining unlabeled samples, namely the beginning of the second wave. *Best vs. 2nd* is more robust against this issue.

3) Runtime: In practice, using structured perceptron for model update yields pleasant runtime. Across iterations it requires (stably) less than 9 seconds to perform model update and uncertainty computation. We consider this a tolerable delay. The final max-margin structured learning run takes between 150 and 200 seconds. Note that this runtime is dependent on the hardware specification of the computer because the underlying solver CPLEX can run the branch-and-bound ILP algorithm in parallel. We used a 2.4 GHz Intel Xeon machine with 12 cores.

4.3 Performance of Combined Learning

We discussed that the purpose of active learning is to retrieve informative training samples while the truly useful model has to be learned via regularized max-margin learning. Table 8 shows the result of this combined learning strategy (CL) using 17% (viz. the stopping point by the convergence measure), 30% and 40% of training samples, compared against the active learning (AL) out-

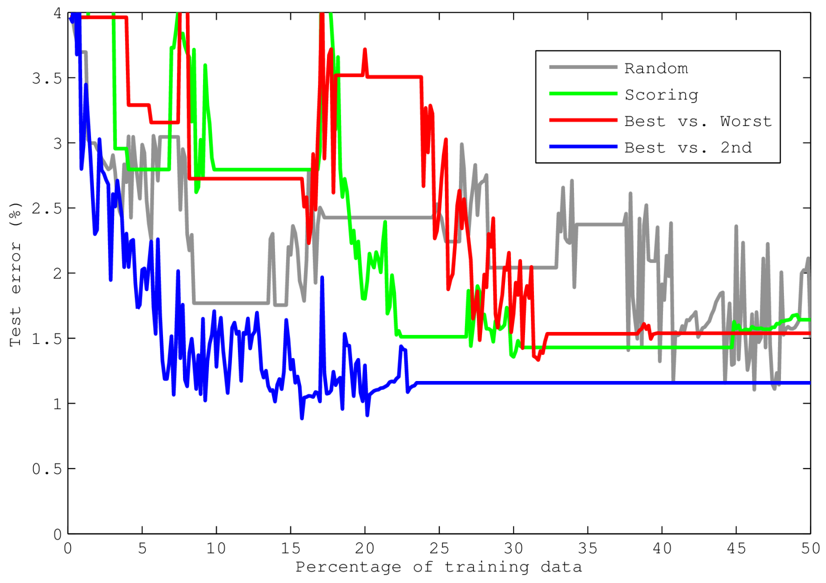

Figure 13: Comparison of uncertainty measure: test error vs. percentage of training data.

put. This affords the following observations. Firstly, using the same amount of training samples, regularized max-margin learning generally improves the output of active learning. Secondly, *Best vs. 2nd* performs better than the other uncertainty measures. Finally (and most importantly), using *Best vs. 2nd* as uncertainty measure and using only 17% of the training samples, we can train a tracking model as competent as the baseline model learned from all samples (last line, Table 8).

4.4 Hyperparameter Optimization

Here we discuss the selection of key hyperparameters used in the regularized max-margin structured learning.

Table 8: Evaluation of Combined Learning – Unit %

	17%		30%		40%	
Measure	AL	CL	AL	CL	AL	CL
Random	1.77	1.66	2.14	1.53	2.43	1.31
Scoring	3.72	1.78	2.79	1.73	1.80	1.11
Best vs. Worst	2.73	2.23	2.73	3.06	3.72	1.36
Best vs. 2nd	1.33	**1.08**	1.26	1.06	1.29	1.09
Baseline	1.07					

First, we optimize the regularization parameter λ via cross validation (5-fold). It turned out that the regularization paths [47] for training with full samples and training with patchified ones are quite distinct (Fig. 14). In practice, we chose $\lambda = 1$ for the former and $\lambda = 10^{-3}$ for the later.

Second, the approximation gap ϵ controls the precision of approximating the learning objective function with piece-wise linear lower bounds (see Fig. 4 and [35]). A lower value means higher precision yet also more computation time (see the embedded figure in Fig. 15 about runtime). We optimize this parameter via empirical tests on a holdout validation dataset (MC4 in this case). As Fig. 15 shows, $\epsilon = 10^{-3}$ is sufficient for both training settings and any higher precision does not increase the test performance.

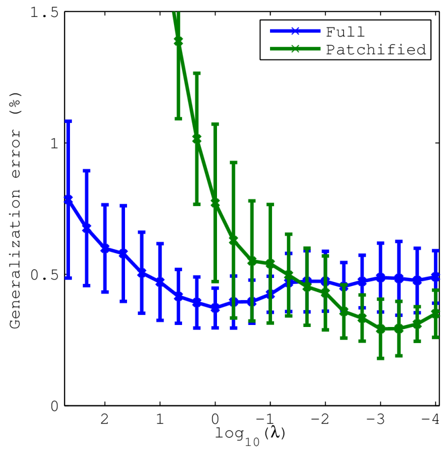

Figure 14: Generalization error vs. regularization parameter λ.

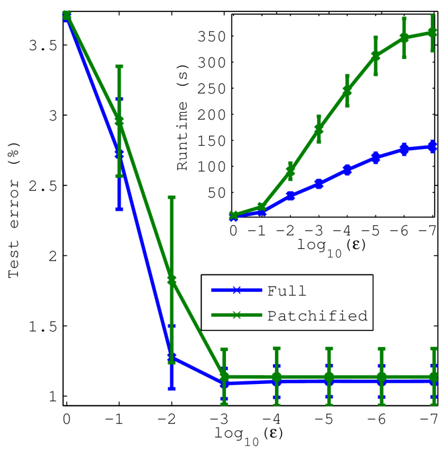

Figure 15: Test error vs. approximation gap ϵ.

4.5 Additional Results

For other results such as sensitivity to training data size and sparse feature selection via $\boldsymbol{L_1}$ norm, please refer to the **supporting document** or [1].

5 Discussions

As all detection/segmentation based tracking, our approach also relies on the quality of segmentation, and we consider its major limitations as follows. Firstly, it cannot recover missing detections. This can be addressed by, for example, extending the technique from [48] which is a global model covering the *entire* sequence. Our learning approach can be adopted to learn this global tracking model, yet this can be prohibitively expensive. A more viable strategy is to train on pairwise models as in this paper, yet perform the tracking globally using the global model. Secondly, our model cannot handle overly segmented objects. This can be alleviated by improving the segmentation. However, a single segmentation cannot always suffice. For example, tuning the segmentation towards less over-segmentation may lead to more under-segmentation. A better solution is to use multiple segmentations that are complementary to each other (e.g. from multiple scales), and model the selection of segmentations jointly with the tracking.

6 Conclusions & Future Work

We present a new cell tracking scheme that uses many expressive features and comes with a structured learning framework to train the larger number of parameters involved. We further propose an active learning approach for efficient training data retrieval that, empirically, reduces the annotation cost to only 17%. Comparison to related methods shows that this learning scheme brings significant improvements in performance and usability.

Acknowledgment

We are very grateful for partial financial support from the CellNetworks Cluster (EXC81), FORSYS ViroQuant (0313923), SBCancer, DFG (GRK 1653) and the Enable fund of the University of Heidelberg. We also thank Jean-Karim Heriche from EMBL (Heidelberg) for providing Mitocheck datasets and Christoph Klein (University of Heidelberg) for ground truth annotation. We thank all reviewers for their insightful and constructive comments.

References

[1] X. Lou and F. A. Hamprecht, "Structured Learning for Cell Tracking," in *Neural Information Processing Systems (NIPS)*, 2011, pp. 1296–1304.

[2] E. Meijering, O. Dzyubachyk, I. Smal, and W. A. van Cappellen, "Tracking in cell and developmental biology," *Seminars in Cell & Developmental Biology*, vol. 20, no. 8, pp. 894 – 902, 2009.

[3] T. Kanade, Z. Yin, R. Bise, S. Huh, S. E. Eom, M. Sandbothe, and M. Chen, "Cell Image Analysis: Algorithms, System and Applications," in *IEEE Workshop on Applications of Computer Vision (WACV)*, 2011.

[4] V. Abraham, D. Taylor, and J. Haskins, "High content screening applied to large-scale cell biology," *Trends in Biotechnology*, vol. 22, no. 1, pp. 15–22, 2004.

[5] A. K. Hadjantonakis, M. E. Dickinson, S. E. Fraser, and V. E. Papaioannou, "Technicolour transgenics: imaging tools for functional genomics in the mouse," *Nature Reviews Genetics*, vol. 4, no. 8, pp. 613–625, 2003.

[6] Z. Bao, J. I. Murray, T. Boyle, S. L. Ooi, M. J. Sandel, and R. H. Waterston, "Automated cell lineage tracing in Caenorhabditis elegans," *Proceedings of the National Academy of Sciences*, vol. 103, no. 8, pp. 2707–2712, 2006.

[7] P. J. Keller, A. D. Schmidt, J. Wittbrodt, and E. H. K. Stelzer, "Reconstruction of zebrafish early embryonic development by scanned light sheet microscopy," *Science*, vol. 322, no. 5904, p. 1065, 2008.

[8] T. Schroeder, "Long-term single-cell imaging of mammalian stem cells," *Nature Methods*, vol. 8, no. 4s, pp. S30–S35, 2011.

[9] J. W. Young, J. C. W. Locke, A. Altinok, N. Rosenfeld, T. Bacarian, P. S. Swain, E. Mjolsness, and M. B. Elowitz, "Measuring single-cell gene expression dynamics in bacteria using fluorescence time-lapse microscopy," *Nature Protocols*, vol. 7, no. 1, pp. 80–88, 2011.

[10] A. Yilmaz, O. Javed, and M. Shah, "Object Tracking: A Survey," *ACM Computing Surveys*, vol. 38, no. 4, 2006.

[11] G. Li, T. Liu, A. Tarokh, J. Nie, L. Guo, A. Mara, S. Holley, and S. T. C. Wong, "3D cell nuclei segmentation based on gradient flow tracking," *BMC Cell Biology*, vol. 8, no. 1, 2007.

[12] Y. Al-Kofahi, W. Lassoued, W. Lee, and B. Roysam, "Improved Automatic Detection and Segmentation of Cell Nuclei in Histopathology Images," *IEEE Transactions on Biomedical Engineering*, vol. 57, no. 4, pp. 841–852, 2010.

[13] X. Lou, U. Köthe, J. Wittbrodt, and F. A. Hamprecht, "Learning to Segment Dense Cell Nuclei with Shape Prior," in *IEEE Conference on Computer Vision and Pattern Recognition (CVPR)*, 2012, pp. 1012–1018.

[14] A. Dufour, V. Shinin, S. Tajbakhsh, N. Guillen-Aghion, J. C. Olivo-Marin, and C. Zimmer, "Segmenting and Tracking Fluorescent Cells in Dynamic 3-D Microscopy With Coupled Active Surfaces," *IEEE Transactions on Image Processing*, vol. 14, no. 9, pp. 1396–1410, 2005.

[15] K. Li, E. D. Miller, M. Chen, T. Kanade, L. E. Weiss, and P. G. Campbell, "Cell population tracking and lineage construction with spatiotemporal context," *Medical Image Analysis*, vol. 12, no. 5, pp. 546–566, 2008.

[16] O. Dzyubachyk, W. A. van Cappellen, J. Essers, W. J. Niessen, and E. Meijering, "Advanced Level-Set-Based Cell Tracking in Time-Lapse Fluorescence Microscopy," *IEEE Transactions on Medical Imaging*, vol. 29, no. 3, pp. 852–867, 2010.

[17] I. Smal, K. Draegestein, N. Galjart, W. Niessen, and E. Meijering, "Particle Filtering for Multiple Object Tracking in Dynamic Fluorescence Microscopy Images: Application to Microtubule Growth Analysis," *IEEE Transactions on Medical Imaging*, vol. 27, no. 6, pp. 789–804, 2008.

[18] D. Padfield, J. Rittscher, and B. Roysam, “Coupled minimum-cost flow cell tracking for high-throughput quantitative analysis,” *Medical Image Analysis*, vol. 15, no. 4, pp. 650–668, 2011.

[19] F. Li, X. Zhou, J. Ma, and S. Wong, “Multiple Nuclei Tracking Using Integer Programming for Quantitative Cancer Cell Cycle Analysis,” *IEEE Transactions on Medical Imaging*, vol. 29, no. 1, pp. 96–105, 2010.

[20] X. Lou, F. O. Kaster, M. S. Lindner, B. X. Kausler, U. Köthe, H. Jänicke, B. Höckendorf, J. Wittbrodt, and F. A. Hamprecht, “DELTR: Digital Embryo Lineage Tree Reconstructor,” in *IEEE International Symposium on Biomedical Imaging: From Nano to Macro (ISBI)*, 2011, pp. 1557–1560.

[21] S. Avidan, “Ensemble Tracking,” in *IEEE Conference on Computer Vision and Pattern Recognition (CVPR)*, 2005, pp. 494–501.

[22] H. Grabner and H. Bischof, “On-line Boosting and Vision,” in *IEEE Conference on Computer Vision and Pattern Recognition (CVPR)*, 2006, pp. 260–267.

[23] M. D. Breitenstein, F. Reichlin, B. Leibe, E. Koller-Meier, and L. V. Gool, “Robust Tracking-by-Detection using a Detector Confidence Particle Filter,” in *IEEE International Conference on Computer Vision (ICCV)*, 2009, pp. 1515–1522.

[24] C.-H. Kuo, C. Huang, and R. Nevatia, “Multi-Target Tracking by On-Line Learned Discriminative Appearance Models,” in *IEEE Conference on Computer Vision and Pattern Recognition (CVPR)*, 2010, pp. 685–692.

[25] B. Zhong, H. Yao, S. Chen, R. Ji, X. Yuan, S. Liu, and W. Gao, “Visual Tracking via Weakly Supervised Learning from Multiple Imperfect Oracles,” in *IEEE Conference on Computer Vision and Pattern Recognition (CVPR)*, 2010, pp. 1323–1330.

[26] X. Wang, G. Hua, and T. X. Han, “Discriminative Tracking by Metric Learning,” in *European Conference on Computer Vision (ECCV)*, 2010, pp. 200–214.

[27] Y. Freund, R. Iyer, R. E. Schapire, and Y. Singer, “An Efficient Boosting Algorithm for Combining Preferences,” *Journal of Machine Learning Research*, vol. 4, pp. 933–969, 2003.

[28] Y. Li, C. Huang, and R. Nevatia, “Learning to Associate: HybridBoosted Multi-Target Tracker for Crowded Scene,” in *IEEE Conference on Computer Vision and Pattern Recognition (CVPR)*, 2009, pp. 2953–2960.

[29] B. Yang, C. Huang, and R. Nevatia, “Learning Affinities and Dependencies for Multi-Target Tracking using a CRF Model,” in *IEEE Conference on Computer Vision and Pattern Recognition (CVPR)*, 2011, pp. 1233–1240.

[30] B. Yang and R. Nevatia, "An online learned CRF model for multi-target tracking," in *IEEE Conference on Computer Vision and Pattern Recognition (CVPR)*, 2012, pp. 2034–2041.

[31] R. Yan, J. Yang, and A. Hauptmann, "Automatically labeling video data using multi-class active learning," in *IEEE Conference on Computer Vision and Pattern Recognition (CVPR)*, 2003, pp. 516–523.

[32] I. Tsochantaridis, T. Joachims, T. Hofmann, and Y. Altun, "Large Margin Methods for Structured and Interdependent Output Variables," *Journal of Machine Learning Research*, vol. 6, no. 2, pp. 1453–1484, 2006.

[33] T. S. Caetano, J. J. McAuley, L. Cheng, Q. V. Le, and A. J. Smola, "Learning Graph Matching," *IEEE Transactions on Pattern Analysis and Machine Intelligence*, vol. 31, no. 6, pp. 1048–1058, 2009.

[34] G. Bakir, T. Hofmann, B. Schoelkopf, A. J. Smola, B. Taskar, and S. Vishwanathan, *Predicting Structured Data*. Cambridge, MA: MIT Press, 2006.

[35] C. H. Teo, S. V. N. Vishwanthan, A. J. Smola, and Q. V. Le, "Bundle methods for regularized risk minimization," *Journal of Machine Learning Research*, vol. 11, pp. 311–365, 2010.

[36] B. Settles, "Active Learning Literature Survey," *Machine Learning*, vol. 15, no. 2, pp. 201–221, 1994.

[37] S. Tong and D. Koller, "Support vector machine active learning with applications to text classification," *The Journal of Machine Learning Research*, vol. 2, pp. 45–66, 2002.

[38] G. Schohn and D. Cohn, "Less is more: Active learning with support vector machines," in *International Conference on Machine Learning (ICML)*. Citeseer, 2000, pp. 839–846.

[39] M. Collins, "Discriminative training methods for hidden markov models: Theory and experiments with perceptron algorithms," in *Meeting of the Association for Computational Linguistics (ACL)*, 2002, pp. 1–8.

[40] L. Bottou, *Large-Scale Kernel Machines*. The MIT Press, 2007.

[41] A. Vlachos, "A stopping criterion for active learning," *Computer Speech & Language*, vol. 22, no. 3, pp. 295–312, 2008.

[42] F. Laws and H. Schätze, "Stopping criteria for active learning of named entity recognition," in *Proceedings of the 22nd International Conference on Computational Linguistics-Volume 1*. Association for Computational Linguistics, 2008, pp. 465–472.

[43] C. Ware, *Information Visualization: Perception for Design*. Morgan Kaufmann, 2004.

[44] S. K. Card, J. D. Mackinlay, and B. Shneiderman, *Readings in Information Visualization: Using Vision to Think.* Morgan Kaufmann, 1999.

[45] M. Held, M. H. A. Schmitz, B. Fischer, T. Walter, B. Neumann, M. H. Olma, M. Peter, J. Ellenberg, and D. W. Gerlich, “CellCognition: time-resolved phenotype annotation in high-throughput live cell imaging,” *Nature Methods*, vol. 7, no. 9, pp. 747–754, 2010.

[46] S. Huh, D. Ker, R. Bise, M. Chen, and T. Kanade, “Automated mitosis detection of stem cell populations in phase-contrast microscopy images,” *IEEE Transactions on Medical Imaging*, vol. 30, no. 3, pp. 586–596, 2011.

[47] T. Hastie, S. Rosset, R. Tibshirani, and J. Zhu, “The entire regularization path for the support vector machine,” *Journal of Machine Learning Research*, vol. 5, pp. 1391–1415, 2004.

[48] B. X. Kausler, M. Schiegg, B. Andres, M. Lindner, U. Köthe, H. Leitte, J. Wittbrodt, L. Hufnagel, and F. A. Hamprecht, “A Discrete Chain Graph Model for 3D+T Cell Tracking with High Misdetection Robustness,” in *European Conference on Computer Vision (ECCV)*, 2012, pp. 144–157.